Responses of tropical deep convection to the QBO: cloud-resolving simulations

Ji Nie * and Adam H. Sobel

Columbia University, New York, New York

* *Corresponding author address:* Lamont-Doherty Earth Observatory, Columbia University, 301E Oceanography, 61 Route 9W, Palisades, NY 10960.

E-mail: jn2460@columbia.edu

ABSTRACT

Observational studies suggest that the stratospheric quasi-biennial oscillation (QBO) can modulate tropical deep convection. We use a cloud-resolving model with a limited domain, representing a convective column in the tropics, to study the mechanisms of this modulation. The large-scale circulation is parameterized using the weak temperature gradient (WTG) approximation, under which the parameterized large-scale vertical motion acts to relax the horizontal mean temperature towards a specified reference profile. Temperature variations typically seen in easterly and westerly phases are imposed in the upper troposphere and lower stratosphere of this reference profile. The responses of convection are studied over different sea surface temperatures, holding the reference temperature profile fixed. This can be thought of as studying the response of convection to the QBO over different "relative SST", and also corresponds to different equilibrium precipitation rates in the control simulation. The equilibrium precipitation rate shows slight increases in response to an QBO easterly phase temperature perturbation over small SST anomalies, and strong decreases over large SST anomalies, and vice versa for the QBO westerly phase perturbation. A column moist static energy budget analysis reveals that the QBO modulates the convective precipitation through two pathways: it changes the high cloud properties and thus the column radiative cooling, and it alters the shape of the large-scale vertical motion and thus the efficiency of energy transport by the large-scale flow. The non-monotonicity of the QBO influence on precipitation with respect to SST results from the competition of these two effects.

1. Introduction

The quasi-biennial oscillation (QBO) is the dominant mode of interannual variability in the tropical stratosphere. It is a quasi-periodic oscillation in which the zonal wind in the equatorial stratosphere switches between easterlies and westerlies with a mean period of about 28 months. Consistent with thermal wind balance, the QBO zonal winds are associated with anomalous meridional circulations and temperature anomalies (e.g. Plumb and Bell 1982). The downward-propagating zonal wind and temperature anomalies extend to the upper troposphere and alter the tropical tropopause height (e.g. Huesmann and Hitchman 2001). There is evidence that the QBO modulates tropical deep convection, as shown by observational analyses showing different anomalies in outgoing longwave radiation (OLR) (Collimore et al. 2003; Huang et al. 2012), high cloud activity (Collimore et al. 2003), and precipitation (Liess and Geller 2012) in tropical deep convective regions during different QBO phases. This modulation, although its magnitude is modest, is a key link in theories of connections between the QBO and tropical tropospheric phenomena such as the the El Niño-Southern Oscillation (ENSO) phenomenon (e.g. Gray et al. 1992; Taguchi 2010, Yuan et al. 2014), the monsoons (e.g. Claud and Terry 2007) and tropical cyclones (e.g. Gray 1984). In these theories, deep convection is influenced by QBO-induced variations in the state of the lower stratosphere and upper troposphere. The QBO-induced convection anomalies may then feed back to stratosphere dynamics by, for example, altering water vapor transport (e.g. Danielsen 1982).

Some previous studies have suggested that the QBO modulates tropical deep convection by perturbing the static stability near the tropopause (e.g. Reid and Gage 1985; Gray et al. 1992; Giorgetta et al. 1999; Garfinkel and Hartmann 2011). Specifically, during the QBO easterly (QBOE) phase, cold temperature anomalies near the tropopause destabilize the troposphere and encourage the development of deep convection. During the QBO westerly (QBOW) phase, the opposite situation holds. Other studies have hypothesized that the QBO zonal winds themselves may play a role in affecting deep convection; strong QBO wind shear

may disrupt the coherent structure of convective plumes and shear off high convective clouds (Gray et al. 1992; Collimore et al. 2003). Based on conventional observations that deeper convection is usually associated with stronger precipitation, these hypotheses further include suggestions that the QBO-induced enhancement of convection in the upper troposphere leads to increases of latent heat release that drive large-scale circulation anomalies.

Here we study this problem using a cloud resolving models (CRM). We explicitly resolve deep convection in a limited domain with relatively high resolution, and parameterize the large-scale circulation (e.g. Sobel and Bretherton 2000; Raymond and Zeng 2005; Kuang 2008; Wang and Sobel 2011; Romps 2012). This approach allows a more accurate representation of convective physics compared to models in which convection is parameterized. At the same time, it allows a plausible representation of the interaction of convection with the large-scale circulation, allowing the occurrence and intensity of convection to vary dynamically and avoiding the artificial constraint that results from approaches in which the large-scale circulation is held fixed (e.g., Mapes 1997; Sobel and Bretherton 2000). There are different ways of parameterizing large-scale motions that are similar in spirit but different in detail (e.g. Sobel and Bretherton 2000; Mapes 2004; Kuang 2007). In this study we apply the weak temperature gradient (WTG) approximation method, which has been used in a number of numerical studies (e.g. Sobel and Bretherton 2000; Raymond and Zeng 2005; Raymond and Sessions 2007; Wang and Sobel 2011; Wang et al. 2013; Emanuel et al. 2014; Anber et al. 2014).

The goal of this paper is to investigate the responses of tropical deep convection to QBO-like temperature anomalies. We also examine the dependence of such responses to the background state, as controlled by imposed anomalies in relative sea surface temperature (SST) which cause the degree of convective activity in the the control climate (before QBO influence) to vary. Section 2 introduces the cloud resolving models, the WTG approximation, and the experiment design. In section 3, we show that the responses of convection to the QBO in simulation results are qualitatively consistent with observations in many aspects.

We show that the QBO precipitation anomalies depends non-monotonically on relative SST, which have not been carefully examined before yet are found in observations and GCM results in qualitatively similar way. Using moist static energy budget analyses, the non-monotonic dependence on relative SST is explained as a result of competition between the effects of radiation anomalies and of large-scale motion anomalies. We conclude in section 4.

2. Methodology

a. The could resolving model

Our numerical simulations are performed with the System for Atmospheric Modeling (SAM, Khairoutdinov and Randall 2003) version 6.8.2. SAM has been widely used to simulate convective systems over a large range of spatial scales (e.g. Khairoutdinov et al. 2009; Kuang 2011; Nie and Kuang 2012a). It solves the anelastic equations of motion on fully staggered Arakawa C grids. There are six classes of hydrometeors in the microphysics schemes: water vapor, cloud liquid, cloud ice, snow, rain, and graupel. The interactive radiation scheme is adopted from the National Center for Atmospheric Research Community Climate Model (Kiehl et al. 1998), and calculates the longwave and shortwave radiation fluxes using the simulated hydrometeors in each individual grid column. A constant solar insolation of 408 W/m^2 is imposed at the top of the atmosphere, thus neither the diurnal nor seasonal cycle is included in the simulations. The surface fluxes are interactively computed using Monin-Obukhov similarity theory. The horizontal mean horizontal winds are relaxed to zero with a time scale of 6 hours. A Newtonian damping is applied in a layer from 22 km to 32 km (the domain top) to absorb the upward-propagating gravity-wave energy.

All experiments in this study are carried out on a spatial domain of 128 km $\times$ 128 km $\times$ 32 km over an ocean surface with doubly periodic lateral boundary conditions. Earths rotation effects are not considered (Coriolis parameter $f = 0$). The horizontal resolution is

2 km. There are 76 stretched vertical levels with a grid spacing increasing smoothly from 75 m near the surface to 500 m above 3000 m. In order to better resolve the convective and radiative processes near the tropopause, following Blossey et al. (2010), we use refined vertical grids with a grid spacing of 250 m between 11 km and 20 km.

b. The weak temperature gradient approach

In this study, large-scale vertical motions are parameterized using the weak temperature gradient (WTG) approximation (e.g. Sobel and Bretherton 2000; Raymond and Zeng 2005). The WTG approach recognizes the fact that the horizontal temperature gradient in tropical free troposphere is weak due to the efficient removal of local temperature anomalies by gravity waves. It thus approximates the large-scale vertical motion to be what is required to relax the CRM horizontal-mean temperature profile to a reference temperature profile (which may be thought of as the tropical mean, or the mean over some other area much larger than the simulation domain) over a fixed time scale. Mathematically, the WTG approximation is implemented here as

$$W_{wtg}\frac{\partial\overline{\theta_v}}{\partial z} = \frac{\overline{\theta_v} - \theta_{v,ref}}{\tau}, \tag{1}$$

where W_{wtg} is the parameterized large-scale vertical velocity, $\overline{\theta_v}$ is the CRM's horizontally averaged virtual potential temperature, and $\theta_{v,ref}$ is the reference virtual potential temperature. The WTG relaxation time scale, τ, is usually interpreted as the time scale for gravity waves to propagate out of the domain. Unless otherwise stated, τ is set to be 3 hours following Wang and Sobel (2011). Sensitivity experiments to the choice of τ are presented in section 3e. At the end of every CRM time step, W_{wtg} is diagnosed using equation (1). The vertical advection of temperature and moisture by W_{wtg} is then applied uniformly in the horizontal on the CRM during the following time step. In the planetary boundary layer (PBL) where WTG is not applicable, as an ad hoc treatment (Sobel and Bretherton 2000), the large-scale vertical velocity is linearly interpolated between zero at surface and the value

of W_{wtg} derived from (1) at the top of PBL, here specified to be at 1 km height. The resulting large-scale vertical motion field, W_{wtg} as per (1) above the PBL top and the interpolated profile below, is applied to the vertical advection terms for both temperature and moisture. In the case of moisture, this implies a dynamically varying large-scale moisture convergence, so that the rates of precipitation and surface evaporation in statistical equilibrium can differ.

Under WTG applied to the CRM as described above, the resulting dynamical system can be thought of comprising three primary components: convection, radiation, and large-scale vertical motion. Convection depends on column state variables such as temperature, moisture, and surface conditions such as SST (Kuang 2010). The interactive radiation depends on the temperature, moisture, and cloud fields. The large-scale motion (W_{wtg}) is a function only of horizontal-mean temperature, but feeds back to influence the other two components through vertical advection of temperature and moisture.

c. Experiment design

To begin with, we present a representative climatological mean tropical temperature sounding (Fig. 1a) and its QBO-associated anomaly (QBOE-QBOW, Fig. 1b). These soundings are from the Singapore station, a benchmark station in QBO studies. The cold temperature anomaly has an amplitude of more than 2 K, peaking at 30 hPa above the cold-point tropopause, and extends down for about 60 hPa below the tropopause (Fig. 1b). Plots from other tropical stations show similar features, as the QBO temperature anomalies are almost uniform within the tropical belt (e.g. Huang et al. 2012).

To establish a base state sounding for the model, the CRM is run to radiative-convective equilibrium (RCE) without WTG (fixed $W_{wtg} = 0$) over a constant SST of 301 K. The resulting RCE temperature profile (T_{rce}, Fig. 1c) reproduces the main characteristics of the tropical sounding in Fig. 1a, although its tropopause height is slightly lower. In the following experiments, T_{rce} (or the same profile converted to virtual potential temperature, $\theta_{v,ref}$ to fit equation (1)), rather than the observed tropical mean temperature, is set as the basic WTG

reference profile because of its better model self-consistency.

Three sets of experiments, corresponding to the QBO neutral phase (QBON) or climatological mean, easterly phase (QBOE), and westerly phase (QBOW), are performed. The QBON group includes 7 experiments, each run over a relative SST (ΔSST) varying from 0.5 K to 4 K with an interval of 0.5 K. In these experiments, the WTG reference profile is held fixed, in all cases set to be T_{rce} described in the previous paragraph (i.e. $T_{ref,QBON} = T_{rce}$). We assume that only deep convection will be sensitive to the QBO anomalies given their high altitude; thus the states over negative ΔSST, which feature either shallow convection only or (for small negative values of ΔSST) weak deep convection, are not considered in this study.

Experiments in the QBOE or QBOW groups differ from experiments in the QBON group by the addition of a negative or positive temperature anomaly to the WTG reference profiles. That is, $T_{ref,QBOE} = T_{rce} + \frac{1}{2}\delta T$, $T_{ref,QBOW} = T_{rce} - \frac{1}{2}\delta T$. Here δT is negative, as shown in Fig. 1d). The idealized δT (Fig. 1d) profile used in the QBOE/QBOW experiments is designed to mimic the observed QBO temperature anomaly (Fig. 1b) in amplitude and altitude of the peak magnitude, relative to the tropopause (adjusting for the slight difference in tropopause height between the control RCE simulation and observations). The observed QBO temperature anomalies in the middle and upper stratosphere (δT signals above 20 km in Fig. 1b) are not included in the idealized δT, because they are too high for convection to reach. The sensitivity of results to the height of the maximum in δT is explored in section 3d.

Each experiment in the three groups is run for 100 days. Model output data from the last 60 days, in which the results are statistically steady, are collected for analysis. Comparing experiments over the same ΔSST but different QBO phases, as imposed through the different reference temperature profiles, allows us to identify the coupled responses of the convection, large-scale circulation and radiation to the QBO. The dependence of these responses on ΔSST is also examined below.

3. Results

a. QBON

Experiments in the QBON group are examined first. In these experiments no QBO temperature anomaly is imposed, and we focus on the changes of convective states with ΔSST.

The response of precipitation to the QBON temperature anomaly is significantly different depending on whether the convection is isolated under RCE or coupled with large-scale motions under WTG. Under RCE, precipitation is constrained to remain nearly constant as ΔSST changes because the convective heating (thus precipitation) has to balance the radiative cooling, which cannot change too much. The free tropospheric temperature is warmer over higher ΔSST, approximately following a moist adiabat connected to an increased PBL temperature. By contrast, under WTG, over positive ΔSST there is an upward W_{wtg} which acts to relax the warmer troposphere temperature back toward T_{ref}. This upward W_{wtg} also vertically transports moisture from lower to upper levels. This implies moisture convergence in the vertical integral, and thus provides additional moisture, in excess of the surface evaporation, that has to be removed by precipitation. As can been seen in Fig. 2a, under WTG the precipitation increases sharply with ΔSST, consistent with previous studies (e.g. Sobel and Bretherton 2000; Ramsay and Sobel 2011; Wang and Sobel 2011).

Quantities that describe characteristics of the three components of the coupled convective system (mass flux in updraft cores for convection, cloud fraction for radiation, and W_{wtg} for large-scale motions) are shown in Fig. 2b-d. Consistent with precipitation, those quantities also increase with ΔSST. The mass flux in updraft cores, defined as positively buoyant grid cells with w greater than 1 m/s, shows typical profiles seen in deep convection (e.g. Khairoutdinov et al. 2009). As ΔSST increases, the changes in the mass flux profile indicate that convection becomes stronger and deeper . There is significant mass flux at the layers above 12.5 km, where δT is imposed on WTG reference profile in QBO perturbed

experiments. These convective plumes can feel the QBO-induced changes of static stability directly. The mass flux at these heights increases with ΔSST, implying that QBO anomalies may have stronger influences on convection over greater ΔSST. This implication is confirmed in the following subsection.

Fig. 2c shows the cloud fraction, defined as a the fraction of grid cells with cloud liquid water greater than 0.01 g/kg or 1 percent of its saturation water vapor. There is a minor peak near the top of the boundary layer and another major peak in the upper troposphere, corresponding to shallow and deep cumulus cloud respectively. Because the radiative warming effects of a high cloud by trapping outgoing longwave generally overcome its cooling effects by reflecting shortwave insolation (keeping in mind that sea surface temperature is fixed, so that the shortwave reduction at the surface has no effect in these simulations), the large high cloud fractions over high ΔSST indicate significant radiative warming to the air column below. Fig. 2d shows that the peak values of W_{wtg} increases with the ΔSST. As convection becomes stronger, the adiabatic cooling by W_{wtg} also has to increase to balance the increased convective heating. These W_{wtg} profiles are qualitatively similar to observed w profiles in deep convective regions (e.g. Back and Bretherton 2006, 2009). They are quite top heavy, however, consistent with previous idealized numerical studies using WTG (Raymond and Sessions 2007; Wang and Sobel 2011).

b. QBOE and QBOW

Next, we examine the equilibrium responses of the coupled convection system to the QBO temperature anomalies. The responses are quite linear in the amplitude of the QBO δT, as determined by experiments in which it is doubled or halved (figures are not shown). The responses are also generally symmetric with the QBO phase. Thus only the differences between the QBOE and QBOW experiments are shown in the rest of the paper.

Fig. 3 plots the differences of the same properties as plotted in Fig. 2, but now showing the difference between the different QBO phases. As can be seen in Fig. 3b, there are

eye-catching positive anomalous peaks of convective updraft core mass flux in the upper troposphere. The enhancement of convection in the upper troposphere is consistent with the previous hypotheses based on the static stability argument (e.g. Gray et al. 1992; Giorgetta 1999). It can also be understood from the point of view that the adjustment of convective plumes produces anomalous convective heating and moistening to remove the initially imposed local temperature perturbations (e.g. Tulich and Mapes 2010; Kuang 2010; Nie and Kuang 2012b). There is also anomalous mass flux in the middle and lower troposphere, however, indicating that the convective adjustments are non-local.

The enhanced convection in the upper troposphere is accompanied by more high cloud, with increases as large as around 10 % (Fig. 3c). This result is consistent with observations of deeper and more extensive high cloud during QBOE in deep convective regions (Collimore et al. 2003). As ΔSST increases, the amplitude of δcld slightly increases and its maximum shifts upward, both contributing to greater anomalous radiative warming of the underlying air, as the emission level is raised and longwave emission is more effectively trapped. The CRM domain-averaged OLR anomalies ($QBOE - QBOW$) range from -4 to -9 $W/m^2/s$ as ΔSST increases from 0.5 to 4 K, comparable with the QBO-associated zonal mean OLR anomalies documented in Collimore et al. (2003).

The responses of W_{wtg} to the QBO shows dipolar patterns centered at the level of 12 km, where W_{wtg} peaks in QBON (comparing Fig. 3d with Fig. 2d). In other words, in QBOE the level of the W_{wtg} maxima shifts upward and the profile becomes more top heavy. The QBO-associated convective heating anomalies are very similar to those of W_{wtg}, because the convective heating and the adiabatic cooling of W_{wtg} approximately balance each other. It is straightforward to understand the upper positive half of δW_{wtg}, because it provides additional adiabatic cooling to relax the column temperature to the colder WTG reference temperature in QBOE. The lower negative half of δW_{wtg} is likely to be related with the non-local convective responses to the cold temperature anomalies above. Kuang (2010) showed that around a reference state the total convective heating and moistening responses are

linear combinations of responses to temperature and moisture perturbations on each level (which are called convective linear response functions, LRF). As can be seen in Fig. 12 of Kuang (2010), for cold temperature anomalies as shown Fig. 1d there is cooling below the perturbed layer, corresponding to the negative δW_{wtg} in Fig. 3d. However, the LRF in Kuang (2010) are constructed based on convections in RCE or with prescribed w. When coupled with WTG, the mean states of convection may drift away enough to modify the response expected baed on the LRFs. The fact that δW_{wtg} increases with ΔSST implies that because of the coupling between convection and large-scale vertical motion, convection is more sensitive to upper-tropospheric temperature perturbations over higher ΔSST.

The percentage change of precipitation in response to the QBO perturbation is shown as a function of ΔSST in Fig. 3a. Contrary to the expectation that enhanced upper tropospheric convection should lead to intensified precipitation (Gray et al. 1992; Giorgetta et al. 1999), δP slightly increases over the first 2.5 K of ΔSST but then sharply decreases to negative values as ΔSST further increases. The non-monotonic dependence of δP on ΔSST is intriguing, and motivates us to ask whether it is consistent with observations or numerical simulations with global models.

Precipitation in GCM studies does not uniformly increase in QBOE. Instead, the precipitation center shifts eastward (in Garfinkel and Hartmann 2011, their Fig. 8) or northward (in Giorgetta et al. 1999, their Fig. 7c-d), while high cloud coverage generally increases over a much larger region. Observational studies also have shown geographic dependence of the QBO δP with both signs (Liess and Galler 2012). We are currently performing an analysis of observation-based precipitation data sets to focus more closely on determining to what extent the response to the QBO depends on relative SST in a way consistent with our simulations. The results of this analysis will be presented in due course.

c. Moist static energy budget analysis

To understand the non-monotonic dependence of δP on ΔSST, an analysis based on the moist static energy (MSE) budget is applied to the model results. Following the original idea proposed by Neelin and Held (1987), different authors have various ways of formulating the budget equation (See review of Raymond et al. 2009). A brief derivation that follows Sobel (2007) is presented here for completeness.

In steady state the vertically integrated temperature equation, phrased in terms of dry static energy ($s = C_pT + gz$, where C_p is the specific heat of dry air, and g is gravitational acceleration), can be written as

$$\langle w\frac{\partial s}{\partial z}\rangle = H + P + R, \tag{2}$$

where H is the surface sensible heat flux, P is the surface precipitation, and R is the vertically integrated radiative heating. $\langle * \rangle$ denotes mass-weighted vertical integral from surface to the top of atmosphere. Similarly, the equation for vertically integrated moist static energy ($h = s + Lq$, where L is the latent heat of vaporization) can be written as

$$\langle w\frac{\partial h}{\partial z}\rangle = H + E + R, \tag{3}$$

where E is the surface latent heat flux. Because h is conserved in moist adiabatic processes, convection only redistributes h vertically, but does not generate or consume h. Equation (2) and (3) state that the balance for $\langle s \rangle$ and $\langle h \rangle$ is between vertical advection of large-scale motion and fluxes at the top and bottom of the column. Horizontal advection terms are neglected in equation (2) and (3) as well as CRM experiments, equivalently assuming that they are much smaller than vertical advection terms or the CRM domain is following a Lagrangian air column. In our experiments, these terms are zero by construction.

Dividing equation (3) by equation (2), one can solve for P:

$$P = \frac{1}{M}(H + E + R) - H - R, \tag{4}$$

where

$$M = \frac{\langle w \frac{\partial h}{\partial z} \rangle}{\langle w \frac{\partial s}{\partial z} \rangle}, \tag{5}$$

is a dimensionless number called the normalized gross moist stability, representing the efficiency of the column moist static energy export by large-scale flow. M is independent of the circulation's amplitude but sensitively depends on the shape of w (e.g., Sobel 2007, Raymond et al. 2009). A more top-heavy w profile is more efficient in exporting MSE, corresponding to larger M and less precipitation under the same MSE forcing ($H + E + R$). The opposite holds for a more bottom-heavy w profile. Many conceptual models of tropical dynamics (e.g. Neelin and Yu 1994; Sobel et al. 2001; Bretherton et al. 2005) set M to be a given constant as "a convenient way of summarizing our ignorance of the details of the convective and large-scale transients" (Neelin and Held 1987). As pointed out by other studies such as Kuang (2011) and also reasoned in section 2b, M (or equivalently w) is actually determined by the interactions between convection and large-scale dynamics. In our MSE budget analysis, M is calculated using model simulated W_{wtg}.

The MSE budget analysis is first applied to the results of the experiments in QBON. Individual MSE source terms (E, H, and R) are shown in Fig. 4a as functions of ΔSST. Surface latent and sensible heat fluxes (E and H) increase with ΔSST. R also increases with ΔSST, as expected, due to the enhanced high cloud radiative warming as seen from Fig. 2c. M decreases with ΔSST (Fig. 4b), mostly due to the fact that W_{wtg} becomes more and more bottom heavy (this is apparent after normalizing W_{wtg} in Fig. 2d, not shown). The decrease of M with ΔSST is more rapid in our results than in results of Wang and Sobel (2011) who used a different model and fixed radiative cooling. The MSE export term $\frac{1}{M}(H+E+R)$ and the term $-(H+R)$ in Equation (4) are shown in Fig. 4c. The MSE export term dominates, mostly due to the decreases of M with ΔSST. The close match shown in Fig. 4c between the rainfall taken directly from the model output and that diagnosed using equation (4) indicates that the MSE budget is well closed.

For each given ΔSST, the imposed QBOE/QBOW atmospheric temperature anomalies

can be viewed as perturbations to the mean state in the corresponding QBON experiment. With linear expansion of equation (4) for different QBO phases over each ΔSST, the precipitation perturbation budget equation can be written as

$$\delta P = (M^{-1} - 1)\delta R + \delta(M^{-1})(H + E + R). \tag{6}$$

In the above equation, we have dropped the δH and δE terms because they are negligible compared to δR, as shown in Fig. 5a-c. The first term on the right hand side is the component of δP due to anomalies of radiative heating. In deep convective regions generally $M < 1$ (Fig. 4b), so positive anomalies of radiative heating are associated with increases in precipitation. The second term on the right hand side is the component of δP due to changes in gross moist stability. With positive MSE forcing, positive anomalies in M result in less precipitation.

The opposite effects of the QBO-associated anomalies in radiation and gross moist stability cause the non-monotonic dependence of δP on ΔSST. During QBOE, there is anomalous radiative heating ($\delta R > 0$ as seen in Fig. 5c) due to the increase in high cloud (Fig. 3c). While δR increases with ΔSST, the dependence becomes weaker when ΔSST is large. The δR term in equation (6) (red line in Fig. 6) contributes to positive precipitation anomalies that increase approximately linearly with ΔSST. By contrast, M becomes larger (equivalently M^{-1} becomes smaller, Fig. 5d) in QBOE due to the upward shift of W_{wtg} peaks as seen in Fig. 3d. The δM term (blue line in Fig. 6) contributes to nonlinear decreases of δP. When ΔSST is high, the reduction in δP due to changes of M dominates the positive δP due to radiation. The curve marked by the black circles, which is the sum of the the δR term and δM term, closely matches the δP of direct model output. It further verifies the perturbation budget equation (6) and the attribution of precipitation anomalies to the combination of transport (gross moist stability) and radiation influences.

d. sensitivity to the penetration depth of QBO temperature anomalies

In this subsection, we perturb the height at which the QBO temperature anomalies is added to the WTG reference profile to test the robustness of our results. This dependence is important to understanding variability in the real atmosphere, as different QBO events have different degrees of penetration into the troposphere (e.g. Huang et al. 2012).

Four pairs of experiments are run over $\Delta SST = 4K$ in QBOE and QBOW; in each the δT (Fig. 1d) profile is shifted in the vertical by $-300m$, $+300m$, $+600m$, $+900m$ (positive refers to an upward shift) respectively, preserving its shape and magnitude. Following similar analyses as in the previous subsections, we examine the responses of the model to the QBO anomalies. Fig. 7a-c shows that the δMF, δcld, and δW_{wtg} have very similar patterns for all cases, indicating that the same mechanism works for all these experiments. However, the amplitude of the response depends sensitively on the height of the δT maximum; they decrease dramatically as δT shifts upward, especially δMF and δW_{wtg}. This is consistent with the finding of Kuang (2010) that the convective LRFs have smaller magnitude for perturbations at higher altitude. The QBO precipitation anomalies diminish as δT shifts upward while they increase significantly as δT shifts downward (Fig. 7d). The reason for this can be seen from Fig. 7c, as δT shifts upward, the amplitude of δW_{wtg} decreases, and so does the δM term in equation (6). At $\Delta SST = 4K$, δP is mainly determined by the δM term, so δP also decreases as the height of δT moves up (Fig. 7d). By contrast, δcld is less sensitive to the height of δT (Fig. 7b), and so is the δR term in equation (6). Following the above argument, we expect that over $\Delta SST < 2.5K$ where δP is determined by the δR term, δP should be less sensitive to the height of δT.

e. sensitivity to τ

The sensitivity of our results to the relaxation time scale τ is explored in this subsection. In WTG, τ can be thought of as proportional to the spatial scale that the limited domain of

CRM represents. All the above experiments have $\tau = 3$ hours, about the time required for a gravity wave with phase speed of 50 m/s to cross a 500 km convective domain. Additional pairs of experiments are performed over $\Delta SST = 4K$ with τ varying from 5 minutes to 6 hours.

The dependence of precipitation (figure not shown) and gross moist stability M on τ (Fig. 8a) are very similar to the results of Wang and Sobel (2011) (their Fig. 13). M maximizes at $\tau = 1hr$, then decreases as τ increases. After examining the results, we found that that the model responds to the QBO is qualitatively similar as τ varies, but the magnitude of the responses depends quantitatively on τ. This magnitude dependence is summarized by the precipitation anomalies, shown in Fig. 8b. δP is only significant when τ is greater than 2 hours, and then increases with τ. The reason can be seen from Fig. 8a; the differences in gross moist stability between the different QBO phases becomes larger as τ increases, as does the contribution of δM to δP.

While more investigation is required to fully understand this dependence, our preliminary analysis agrees with the argument in Kuang (2011): as τ increases (or equivalently the length scale of the convective region increases), the weaker WTG relaxation allows larger temperature anomalies from the reference profile, which are sufficient to affect the convective heating and feed back to the large-scale vertical motion.

The proportional relationship between δP and τ, however, is not expected to hold as τ becomes sufficiently large. As τ approaches infinity, the system return to RCE, in which precipitation is determined by radiative cooling and the coupling between convection and large-scale vertical motion vanishes. In this limit, only small QBO-related precipitation anomaly is expected.

4. Conclusions

We have conducted a set of cloud-resolving numerical experiments in the weak temperature gradient framework to examine the mechanisms by which the QBO influences tropical convection. The results lead us to an interpretation in which the QBO's temperature anomalies exert their influence on the tropical troposphere through interactions between convection, radiation, and large-scale vertical motion. The main findings are summarized as follows.

1. With a QBOE (cold) temperature perturbation in the lowermost stratosphere and uppermost troposphere, the convective mass flux and cloud fraction increase near the tropopause, making the large-scale vertical motion profile more top heavy. The opposite is true for the QBOW (warm) temperature perturbation. These responses increase in magnitude with relative SST, indicating stronger coupling between convection and large-scale motions over the warmest waters.

2. In contrast to the high clouds and mass fluxes, the dependence of precipitation on relative SST is non-monotonic. The QBO precipitation anomalies are the results of a competition between increases due to anomalous radiative heating and decreases due to changes of gross moist stability, the latter resulting from increasing top-heaviness of the vertical motion profile profile. The QBO precipitation anomalies slightly increase over the first 2.5 K of relative SST, where the radiative feedback dominates. They then sharply decrease to negative values as relative SST further increases as the increasing gross moist stability anomalies become more important and overwhelm the radiative feedback.

3. The amplitude of the precipitation response sensitively depends on the depth to which the QBO temperature perturbations can penetrate. The deeper into the troposphere the QBO temperature anomalies can reach, the stronger the response of convection. The dependence of our model results on the WTG relaxation time τ suggests that the responses of deep convection to the QBO are significant only when the length scale of the convective region is greater than several hundred kilometers.

The current study challenges the notion that the enhanced upper troposphere convection

in QBOE leads to more precipitation and stronger large-scale ascent. The simulation results show that rather than generally increasing in all levels, the large-scale vertical motion profile responses to the QBOE perturbation by increasing in the upper troposphere and decreasing below. The responses shifts the vertical motion profiles so that they become more top heavy, thus leading to increasing gross moist stability and decreasing precipitation. The decreasing precipitation overcomes the increases of precipitation due to anomalous radiative heating in regions with high relative SST. There are indications in previous observational studies that these results may be consistent with observations, in that the QBO-related precipitation anomalies are not of a single sign. We are currently conducting an analysis directly motivated by our present numerical results, in order to test the hypothesis of a non-monotonic SST dependence more directly, and will report the results in due course.

Acknowledgments.

The authors thank Wei Yuan for preparation of the tropical sounding data; Marvin A. Geller, Shuguang Wang and Wei Yuan for discussion; Zhiming Kuang for computational resources support. AHS acknowledges support from NSF grant AGS -1008847.

443 REFERENCE:

444 Anber, U., W. Wang and A. Sobel, (2014): Response of atmospheric convection to vertical
445 wind shear: cloud-system-resolving simulations with parameterized large-scale circulation.
446 part I: specified radiative cooling. J. Atmos. Sci., 71, 2976-2993.

447 Back, L. E., and C. S. Bretherton, (2006): Geographic variability in the export of moist
448 static energy and vertical motion profiles in the tropical Pacific. Geophys. Res. Lett., 33,
449 L17810, doi:10.1029/2006GL026672.

450 Back, L. E., and C. S. Bretherton, (2009): A simple model of climatological precipitation
451 and vertical motion patterns over the tropical oceans. J. Clim., 22, 6477-6497.

452 Blossey, P. N., Z. Kuang, and D. M. Romps, (2010): Isotopic composition of water in the
453 tropical tropopause layer in cloud-resolving simulations of an idealized tropical circulation.
454 J. Geophys. Res., 115, D24309, doi:10.1029/2010JD014554.

455 Claud, C., and P. Terray, (2007): Revisiting the possible links between the Quasi-Biennial
456 Oscillation and the Indian Summer Monsoon using NCEP R-2 and CMAP fields. J. Clim.,
457 20, 773-787.

458 Collimore, C. C., D. W. Martin, M. H. Hitchman, A. Huesmann, and D. E. Waliser,
459 (2003): On the relationship between the QBO and tropical deep convection. J. Clim., 16,
460 2552-2568.

461 Danielsen, E. F., (1982): A dehydration mechanism for the stratosphere. Geophys. Res.
462 Lett., 9, 605-608.

463 Emanuel, K., A. A. Wing, and E. M. Vincent, (2014): Radiative-convective instability.
464 J. Adv. Model. Earth Syst., 6, 75-90.

465 Garfinkel, C.I., and D. L. Hartmann, (2011): The Influence of the Quasi-Biennial Oscil-
466 lation on the Troposphere in Winertime in a Hierarchy of Models, Part II: Perpetual Winter
467 WACCM runs. J. Atmos. Sci., 68, 2026-2041.

468 Giorgetta, M. A., L. Bengtsson, and K. Arpe, (1999): An investigation of QBO signals
469 in the east Asian and Indian monsoon in GCM experiments. Clim. Dyn., 15, 435-450.

Gray, W. M., (1984): Atlantic Seasonal Hurricane Frequency. Part I: El Niño and 30 mb Quasi-Biennial Oscillation Influences. Mon. Wea. Rev., 112, 1649-1668.

Gray, W. M., J. D. Scheaffer, and J. A. Knaff, (1992): Influence of the stratospheric QBO on ENSO variability. J. Meteor. Soc. Japan, 70, 975-995.

Huang, B., Z.-Z. Hu, J. L. Kinter III, Z. Wu, and A. Kumar, (2012): Connection of stratospheric QBO with global atmospheric general circulation and tropical SST. Part I: Methodology and composite life cycle. Clim. Dyn., 38, 1-23.

Huesmann, A. S., and M. H. Hitchman, (2001): The stratospheric quasi-biennial oscillation in the NCEP reanalyses: Climatological structures. J. Geophys. Res., 106(D11), 11859-11874, doi:10.1029/2001JD900031.

Khairoutdinov, M. F., and D. A. Randall, (2003): Cloud resolving modeling of the ARM summer 1997 IOP: Model formulation, results, uncertainties, and sensitivities. J. Atmos. Sci., 60, 607-625.

Khairoutdinov, M. F., S. K. Krueger, C.-H. Moeng, P. A. Bogenschutz, and D. A. Randall, (2009): Large-Eddy Simulation of Maritime Deep Tropical Convection. J. Adv. Model. Earth Syst., 1, 15, doi:10.3894/JAMES.2009.1.15.

Kiehl, J. T., J. J. Hack, G. B. Bonan, B. A. Boville, D. L. Williamson, and P. J. Rasch, (1998): The National Center for Atmospheric Research Community Climate Model: CCM3. J. Clim., 11, 1131-1149.

Kuang, Z., (2008): Modeling the interaction between cumulus convection and linear waves using a limited domain cloud system resolving model. J. Atmos. Sci., 65, 576-591.

Kuang, Z., (2010): Linear response functions of a cumulus ensemble to temperature and moisture perturbations and implication to the dynamics of convectively coupled waves. J. Atmos. Sci., 67, 941-962.

Kuang, Z.,(2011): The wavelength dependence of the gross moist stability and the scale selection in the instability of column integrated moist static energy. J. Atmos. Sci., 68, 61-74.

Liess, S., and M. A. Geller, (2012): On the relationship between QBO and distribution of tropical deep convection. J. Geophys. Res., 117, D03108, doi:10.1029/2011JD016317.

Mapes, B.E., (1997): Equilibrium vs. activation controls on large-scale variations of tropical deep convection. The physics and parameterization of moist convection, Kluwer Academic Publishers, Dordrecht, pp 321-358.

Mapes, B. E., (2004): Sensitivities of cumulus-ensemble rainfall in a cloud- resolving model with parameterized large-scale dynamics. J. Atmos. Sci., 61, 2308-2317.

Neelin, J. D., and I. M. Held, (1987): Modeling tropical convergence based on the moist static energy budget. Mon. Wea. Rev., 115, 3-12.

Nie, J. and Z. Kuang, (2012a): Beyond bulk entrainment and detrainment rates: a new framework for diagnosing mixing in cumulus convection. Geophys. Res. Lett. 39, L21803, doi:10.1029/2012GL053992.

Nie, J., and Z. Kuang, (2012b): Responses of Shallow Cumulus Convection to Large-scale Temperature and Moisture Perturbations: a comparison of large-eddy simulations and a convective parameterization based on stochastically entraining parcels. J. Atmos. Sci, 69, 1936-1956.

Plumb, R. A., and R. C. Bell, (1982): A model of the quasi-biennial oscillation on an equatorial beta-plane. Q.J.R. Meteorol. Soc., 108, 335-352.

Ramsay, H. A., and A. H. Sobel, (2011): The effects of relative and absolute sea surface temperature on tropical cyclone potential intensity using a single column model. J. Clim., 24, 183-193.

Raymond, D. J. and X. Zeng, (2005): Modelling tropical atmospheric convection in the context of the weak temperature gradient approximation. Q.J.R. Meteorol. Soc., 131: 1301-1320.

Raymond, D. J., and S. L. Sessions, (2007): Evolution of convection during tropical cyclogenesis. Geophys. Res. Lett., 34, L06811, doi:10.1029/2006GL028607.

Raymond, D. J., S. L. Sessions, A. H. Sobel, and Z. Fuchs, (2009): The Mechanics of

524 Gross Moist Stability. J. Adv. Model. Earth Syst., 1, 9, doi:10.3894/JAMES.2009.1.9.

525 Romps D. M., (2012): Weak Pressure Gradient Approximation and Its Analytical Solu-
526 tions. J. Atmos. Sci., 69, 2835-2845.

527 Reid, G. C., and K. S. Gage, (1985): Interannual variations in the height of the tropical
528 tropopause. J. Geophys. Res., 90, 5629-5635.

529 Sobel, A. H., and C. S. Bretherton, (2000): Modeling tropical precipitation in a single
530 column. J. Clim., 13, 4378-4392.

531 Sobel, A., (2007): Simple models of ensemble-averaged precipitation and surface wind,
532 given the SST. The Global Circulation of the Atmosphere, T. Schneider and A. H. Sobel,
533 Eds., Princeton University Press.

534 Taguchi, M., (2010): Observed connection of the stratospheric quasi-biennial oscillation
535 with El Ninño Southern Oscillation in radiosonde data. J. Geophys. Res., 115: D18120,
536 DOI: 10.1029/2010JD014325.

537 Tulich, S. N, and B. E. Mapes, (2010): Transient Environmental Sensitivities of Explicitly
538 Simulated Tropical Convection. J. Atmos. Sci., 67, 923-940.

539 Wang S., and A. Sobel, (2011): Response of convection to relative sea surface temper-
540 ature: cloud-resolving simulations in two and three dimensions. J. Geophys. Res., 116,
541 D11119, doi:10.1029/2010JD015347.

542 Wang, S., A. H. Sobel, and Z. Kuang, (2013): Cloud-resolving simulation of TOGA-
543 COARE using parameterized large-scale dynamics. J. Geophys. Res. Atmos., 118, 6290-
544 6301.

545 Yuan, W., M. A. Geller and P. T. Love, (2014): ENSO influence on QBO modulations
546 of the tropical tropopause. Q.J.R. Meteorol. Soc., 140:1670-1676.

List of Figures

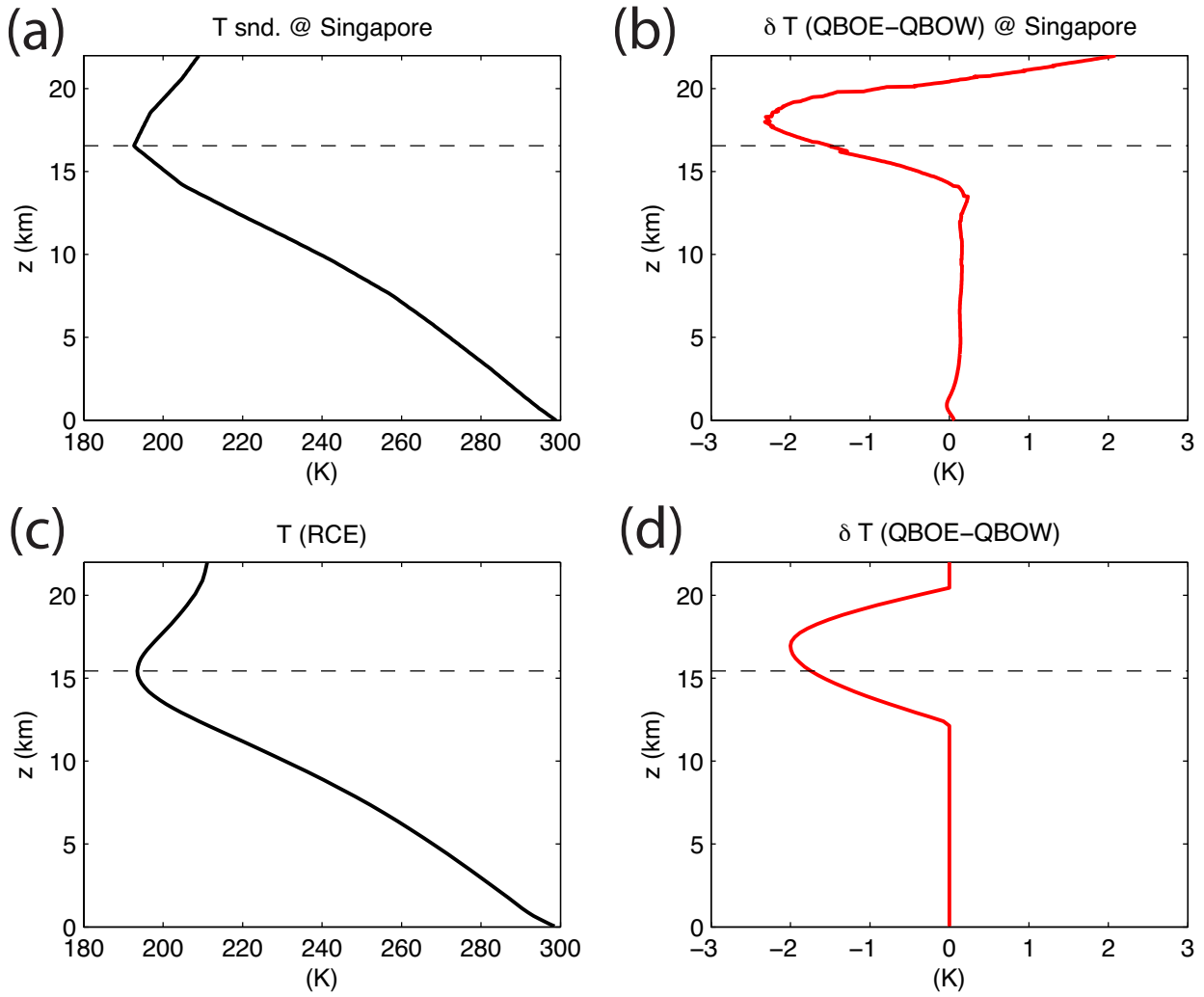

FIG. 1. (a) The climatological mean temperature profile and (b) the QBO temperature anomalies relative to the climatological Singapore station sounding. (c) The RCE temperature profile. (d) The idealized QBO temperature anomalies that are used in the QBOE/QBOW experiments. The horizontal black dash lines indicate the height of the cold-point tropopause.

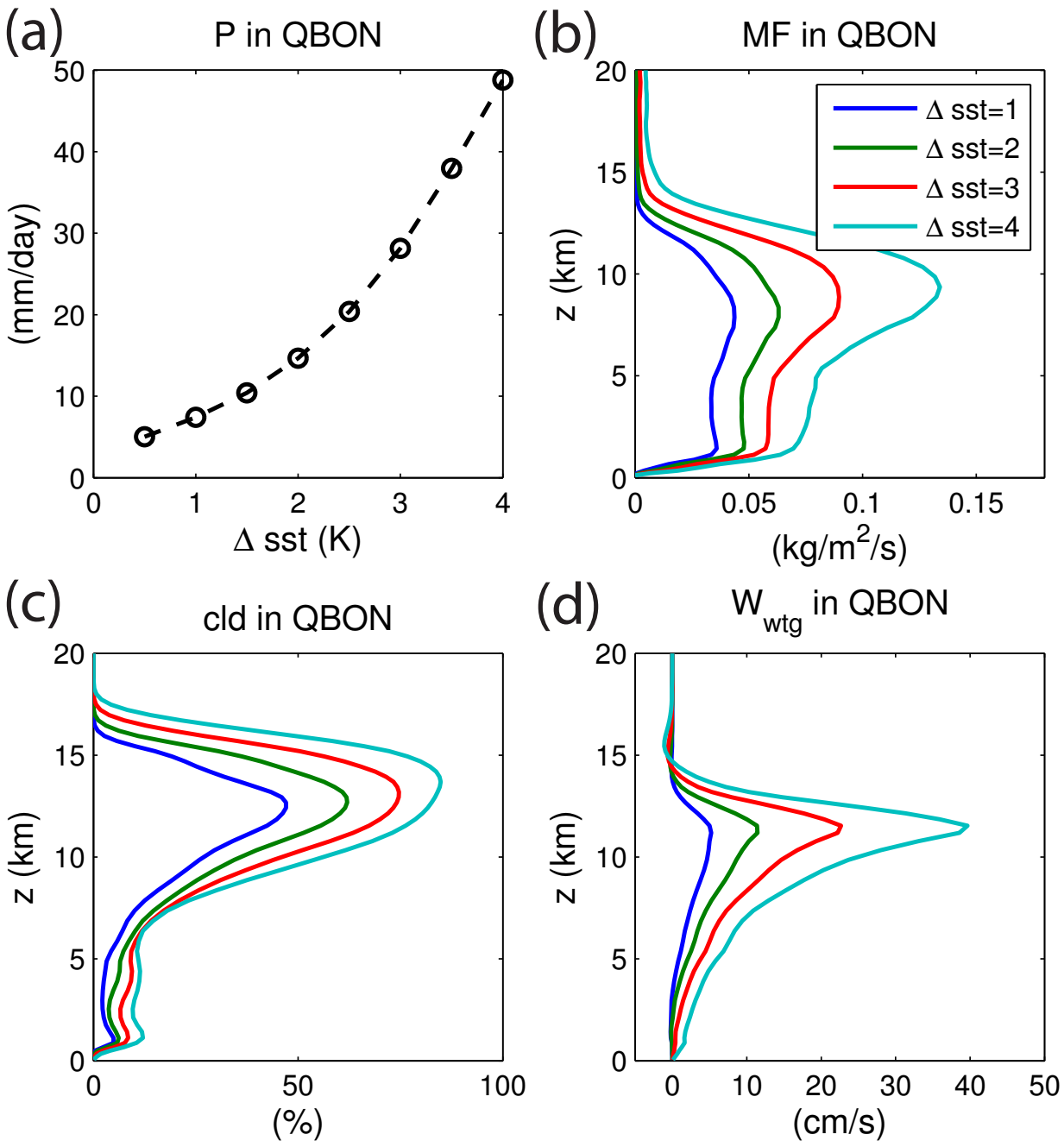

FIG. 2. (a) Precipitation as a function of ΔSST for the QBON experiments. (b)-(d): The vertical profiles of the mass flux in updraft cores, cloud fraction, and W_{wtg} for the QBON experiments with varying ΔSST.

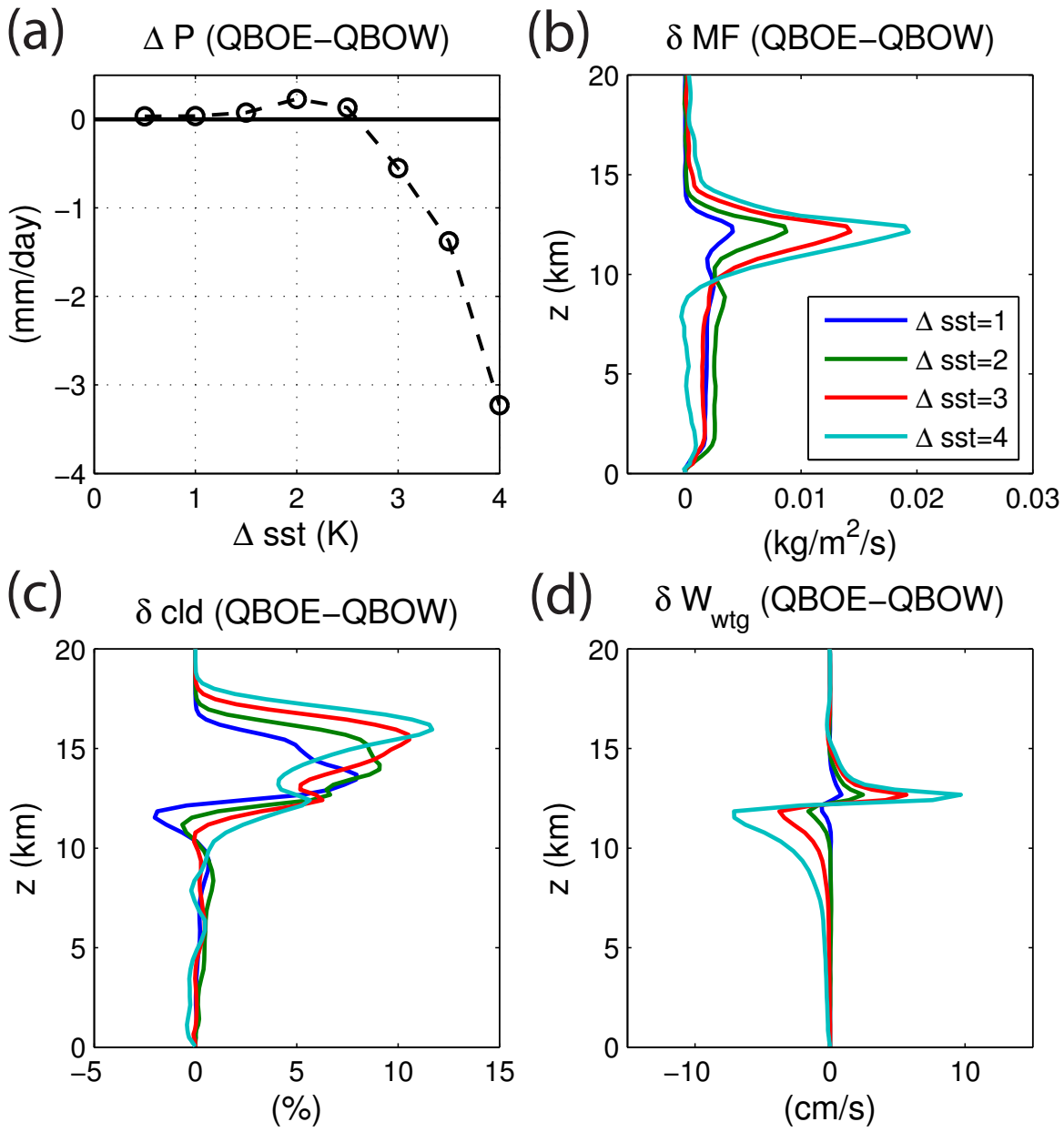

FIG. 3. (a) QBO anomalous precipitation in percentage as a function of ΔSST . (b)-(d): The differences of the mass flux in cloud cores, the cloud fraction, and the W_{wtg} between experiments in the QBOE and QBOW groups.

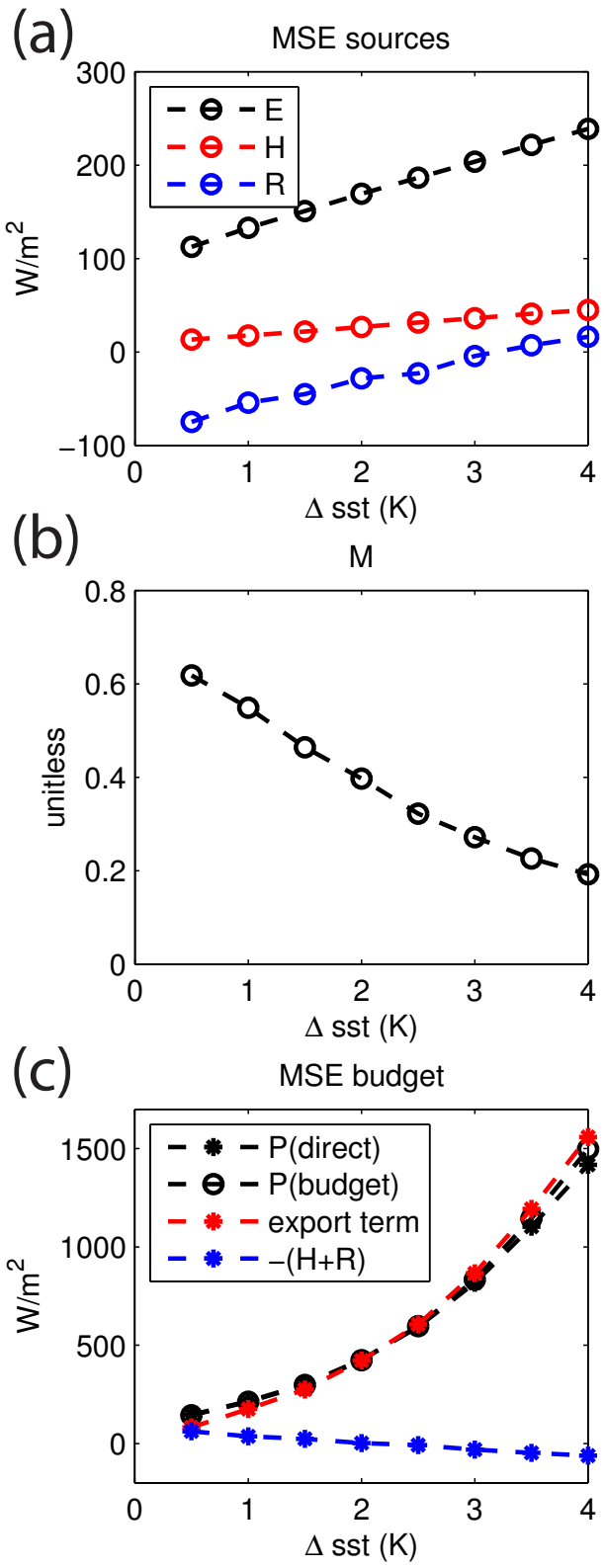

FIG. 4. (a) the moist static energy source terms in equation (4), (b) the gross moist stability M, and (c) moist static energy budget terms as functions of ΔSST. (c) shows the precipitation taken directly from model results and diagnosed from equation (4) in unit of Wm^{-2}, as well as the export term $\frac{1}{M}(H+E+R)$ and the $-(H+R)$ term. All the panels are for the QBON experiments.

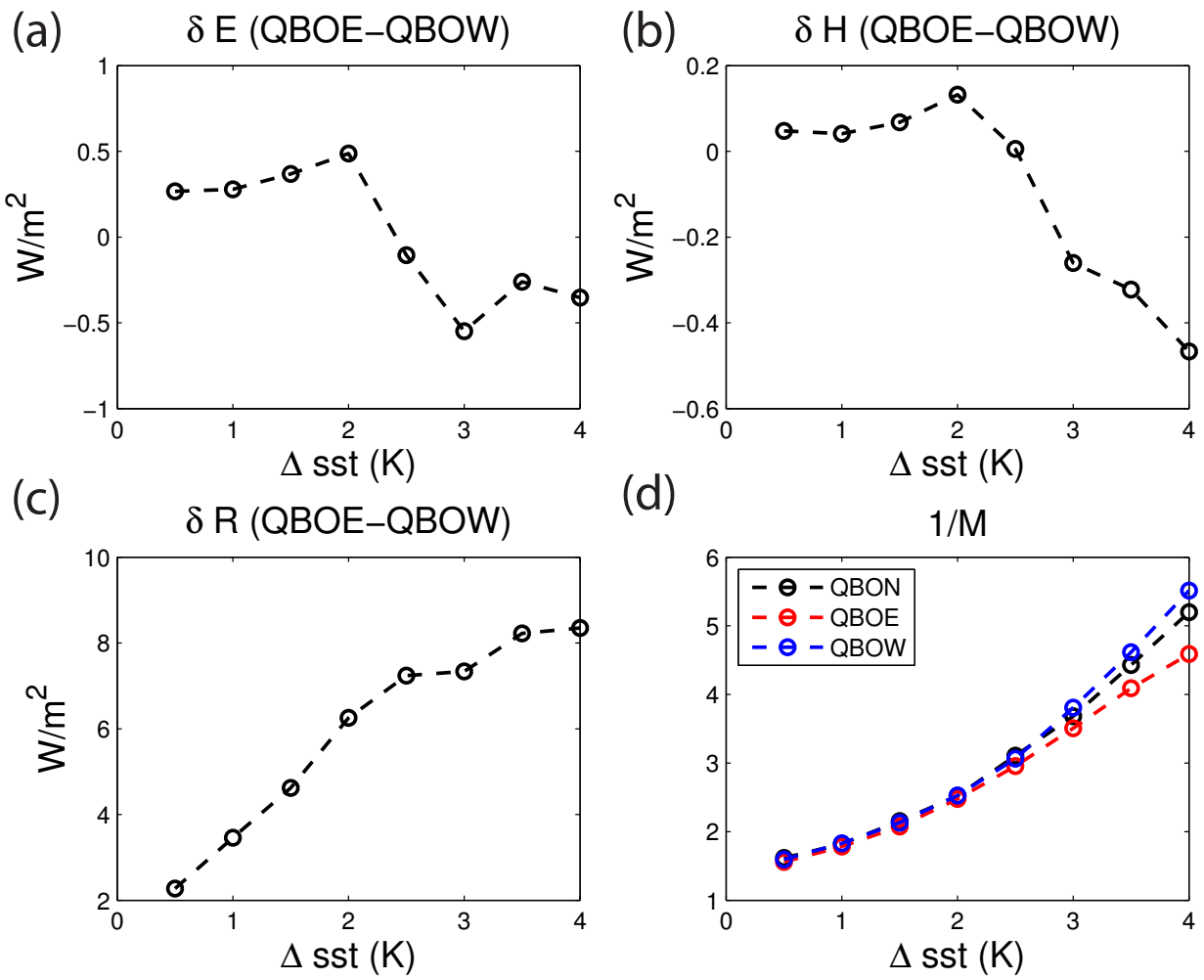

FIG. 5. The anomalies of (a) E, (b) H, and (c) R due to the QBO over varying ΔSST. (d) shows the inverse of M in different QBO phases.

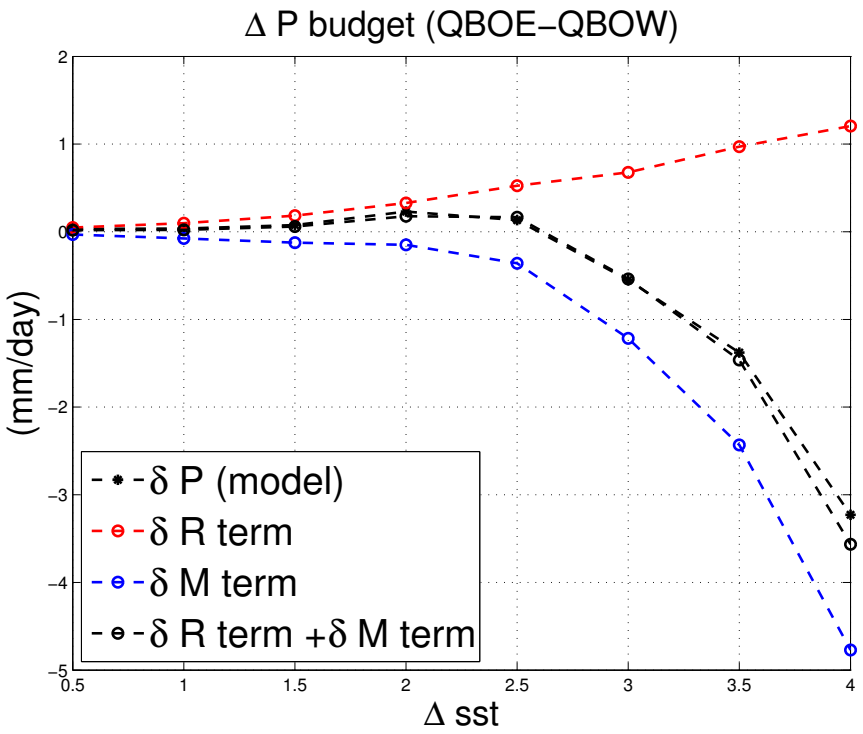

FIG. 6. The δP budget terms of equation (6). The red cycle line is the δR term; the blue cycle line is the δM term; the black cycle line is the sum of δR term and δM term; and the black star line is the δP that comes from model direct output of precipitation.

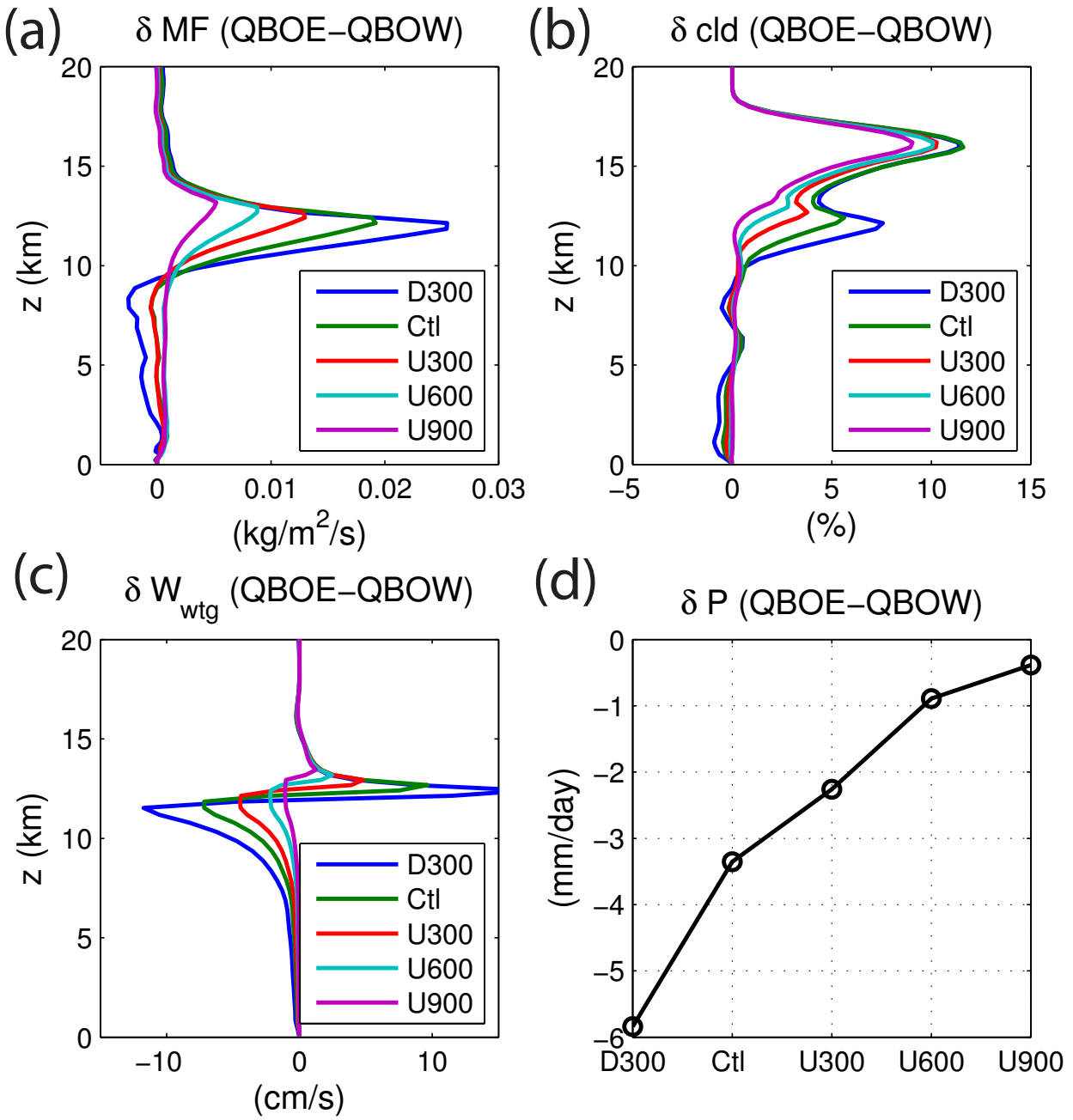

FIG. 7. The (a) δMF, (b) δcld, (c) δW_{wtg}, and (d) δP for experiments with different δT height. "Ctl" is the experiments with δT shown in Fig. 1d. "D300" denotes that δT height is shifted downward for 300 m; "U300", "U600", and "U900" denote that δT height is shifted upward for 300 m, 600 m, and 900 m, respectively. All experiments are run over $\Delta SST = 4K$.

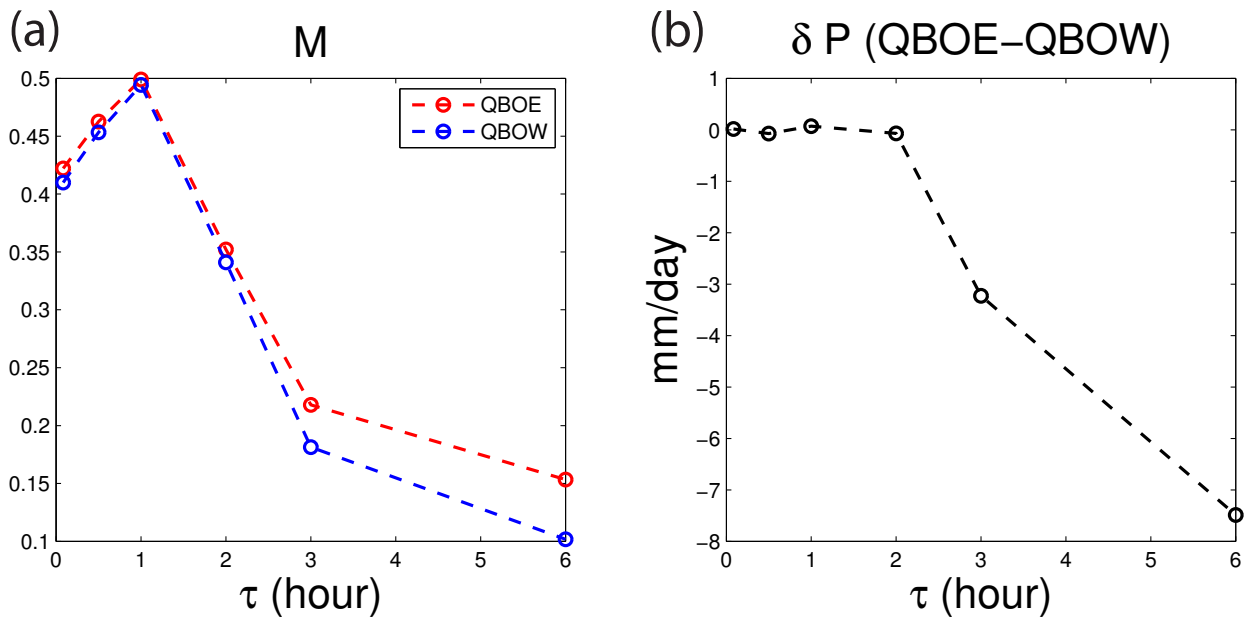

FIG. 8. (a) M as functions of τ in two QBO phases. (b) δP as a function of τ. All experiments are run over $\Delta SST = 4K$.